

Evaporation-Induced Crumpling of Graphene Oxide Nanosheets in Aerosolized Droplets: Confinement Force Relationship

*Wei-Ning Wang, Yi Jiang, Pratim Biswas**

Aerosol and Air Quality Research Laboratory
Department of Energy, Environmental and Chemical Engineering
Washington University in St. Louis
St. Louis, MO 63130, USA

The Journal of Physical Chemistry Letters

*To whom correspondence should be addressed:

Tel: (314) 935-5482; Fax: (314) 935-5464

Email: pbiswas@wustl.edu

Table of Contents

- S1. Extended Experimental Methods
- S2. Derivation of the Confinement Force Equation
- S3. Calculation of Residence Time
- S4. Effect of pH
- S5. Supplementary References

S1. Extended Experimental Methods

Synthesis of Graphene Oxide. The graphene oxide nanosheets were prepared by using the modified Hummers method.¹ Graphite powders (45 μm , Sigma-Aldrich) were used as the raw materials. In this method, 50 ml of concentrated sulfuric acid (H_2SO_4) was added into a beaker containing 2 g of graphite at room temperature. The beaker was cooled to 0°C by using an ice bath. Six gram of potassium permanganate (KMnO_4) was then slowly added to the above mixture while it was allowed to warm to room temperature. The suspension was stirred for 2 h at 35°C . After the suspension was cooled in an ice bath, it was diluted by 350 ml of deionized (DI) water. Then, hydroperoxide aqueous solution (H_2O_2 , 30%) was added until the gas evolution ceased in order to reduce residual permanganate. The suspension was then filtered, washed by DI water, and dried at room temperature for 24 h to obtain brownish graphite oxide powder. The dry graphene oxide powder was redispersed in DI water and sonicated for 3 h to get exfoliated single nanosheets. The suspension was then centrifuged at 10,000 rpm for 30 min and the supernatant was used as the precursor for crumpled graphene oxide preparation. The GO aqueous suspension is stable for months with negligible sedimentation observed (see **Fig. S1** for details). This great stability stems from the mutual columbic repulsion between negatively charged GO surfaces as confirmed by the measured negative zeta potential (-37 mV) (**Fig. S1c**). Functional groups such as epoxides, hydroxyls, and carboxylic groups adorn the surface of GO to render it suspendable in polar solvents. The mass concentration of GO was determined by measuring its optical absorbance using UV-Vis spectra based on the Beer-Lambert law.² A linear relationship between the absorption intensity and the concentration of GO in a wide range has also been observed previously.³ The typical absorption spectra of GO with different mass concentrations were plotted in **Fig. S2a** and the calibration curves are shown in **Fig. S2b**.

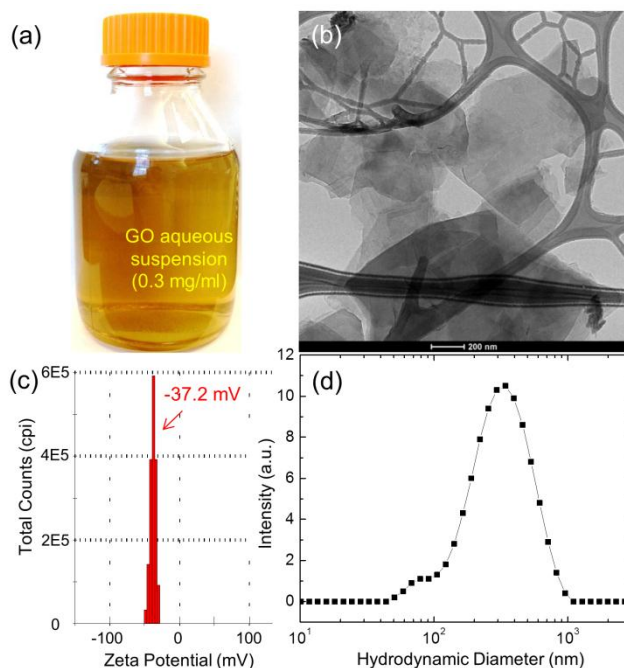


Fig. S1. Representation characterization results of graphene oxide. (a) Photo of GO aqueous suspension, (b) Corresponding TEM image of GO nanosheets, (c) Zeta potential, and (d) intensity-based size distribution measured by DLS.

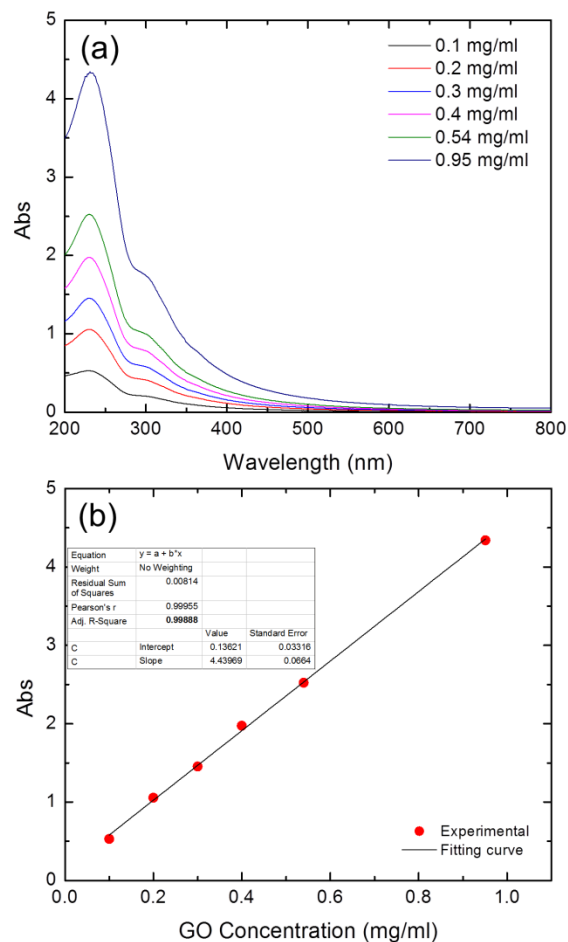


Fig. S2. Mass concentration determination by UV-Vis measurements. (a) Typical UV-Vis absorption spectra of GO aqueous solutions with different concentrations, and (b) the corresponding calibration curve.

Synthesis of Crumpled Graphene Oxide Particles. The crumpled graphene oxide particles were synthesized by a furnace aerosol reactor (FuAR) method, which is schematically shown in **Fig. 1a**. The FuAR consisted of a 6-jet Collision nebulizer (BGI Instruments, Waltham, MA) as the atomizer, an electric furnace, a tubular alumina reactor, a microfiber filter, an air pump, and cooling and gas feeding systems. The schematic diagram of crumpled GO particle formation inside the FuAR is shown in **Fig. 1b**. The precursors were atomized into micrometer-sized droplets by means of the atomizer, and the mist was delivered by air into the tubular alumina reactor (1 m in length and 25 mm in inner diameter) maintained at predetermined temperatures (from room temperature to 1000°C), followed by heating for several seconds. The droplet size (D_d) was controlled by adjusting nebulizer pressure (P_{neb}) and was measured by using an aerodynamic particle sizer (APS, TSI Inc.). Typical droplet size distributions and the geometric mean droplet diameters as a function of P_{neb} were plotted in **Fig. S3**. The results reveal that the droplet sizes decreased monotonously from 3.7 μm at 40 kPa to 2.0 μm at 210 kPa. The droplet sizes of pure water and GO aqueous suspensions ($C = 0.54$ and 0.95 mg/ml) at a certain condition were almost the same due to the similarity of their physical properties. During the

process, the micrometer-sized droplets underwent solvent evaporation, evaporation-driven crumpling of GO nanosheets, and further drying to form the final GO or reduced GO particles. These particles were collected downstream of the reactor using the glass microfiber filter (EPM 2000, Whatman Inc.) for characterization.

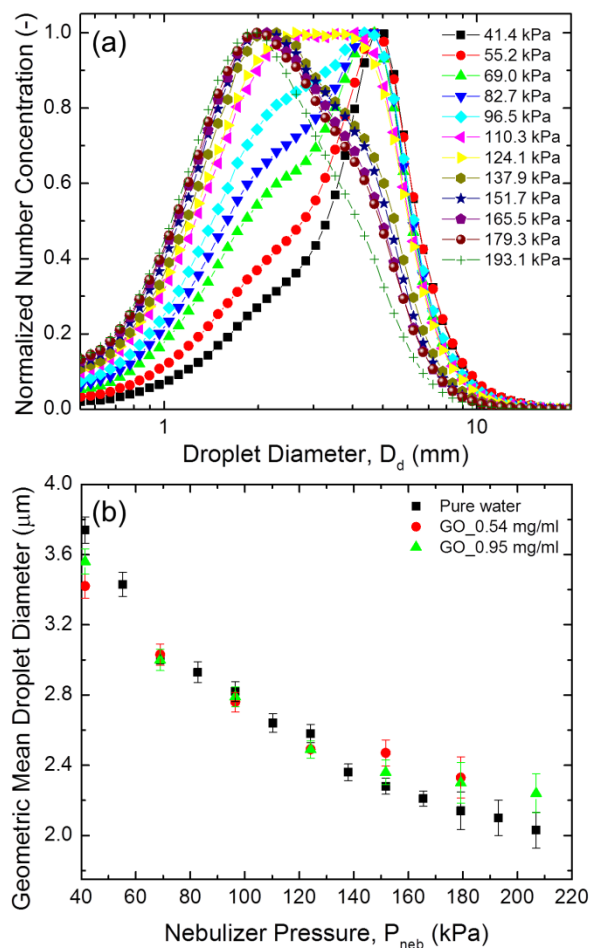


Fig. S3. Droplet size measurements by using aerodynamic particle sizer. (a) droplet size distribution and (b) average droplet diameter as a function of pressure.

Materials Characterization. The morphology and size of the GO samples were examined by transmission electron microscopy (TEM, TecnaiTM Spirit, FEI Co.) and field emission scanning electron microscopy (FESEM, NOVA NanoSEM 230, FEI Co.). The average diameters (geometric mean diameter, D_{pg}) were determined by randomly sampling more than 200 particles from the FESEM images. An example particle size distribution of the crumpled GO particles is shown in **Fig. S4**, from which a peak diameter of around 200 nm is observed for the crumpled GO particles synthesized from a diluted GO suspension. It should be noted that the particle sizes obtained from SEM/TEM images are oftentimes overestimated due to agglomeration of particles caused by sample preparation. The hydrodynamic diameter of suspended GO was also measured using dynamic light scattering (DLS) using Zetasizer Nano ZS system (Malvern Instruments Ltd., Worcestershire, UK) with a measurable size range of 0.3 nm to 10 μm (see **Fig. S1d** for an example). A red laser ($\lambda = 633$ nm) was used as the light source with a scattering angle of 173°.

For each measurement, 3 runs with 14 cycles per run were carried out, and the average values were used. It is noteworthy that the DLS measurement is based on the assumption that all particles are effective spheres and undergo Brownian motion in the solution. Because of the special geometrical structure of GO, it appears that the DLS technique is not quantitatively reliable. Therefore, the DLS analysis presented here should be viewed only as a qualitative indicator to shed light on the pH-dependent aggregation of GO. Online particle size measurements were performed by using a scanning mobility particle sizer (SMPS, TSI Inc.) system, which consists of a differential mobility analyzer (DMA, TSI 3081, TSI Inc.) and a condensation particle counter (CPC, TSI 3025, TSI Inc.). During online measurements, a 0.3 lpm slip-stream of aerosols was drawn into the SMPS system, which measures particle size in the range of 9 ~ 425 nm and particle number concentration up to 10^7 #/cm³. The above size measurements for each sample were performed five times and average data and standard deviations were obtained. The ultraviolet-visible (UV-VIS) spectra analysis was also performed (Cary 100, Varian, Inc., Palo Alto, CA), to check optical properties of GO and determine the mass concentration of GO suspension as shown above (see Fig. S2).

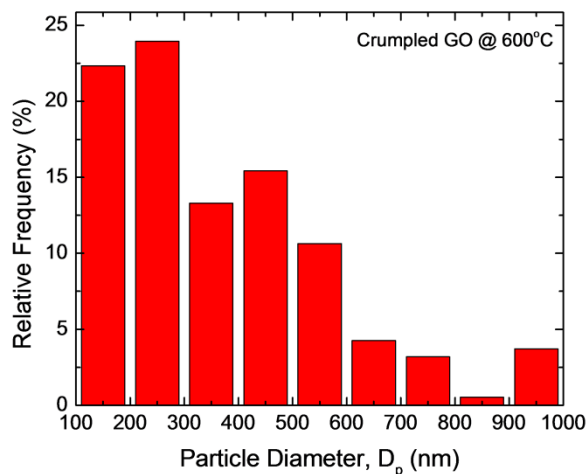


Fig. S4. Particle size distribution of crumpled GO particles synthesized from 0.54 mg/ml GO suspension at 600°C obtained from FESEM images by sampling 200 particles. The peak diameter is around 200 nm.

S2. Derivation of the Confinement Force Equation

The solvent, i.e. water in this work, the evaporation rate of single micrometer-sized droplet at different furnace temperature could be simply calculated according to the follow equation.^{4,5}

$$\kappa = \frac{m_d}{\tau_e} \quad (1)$$

where κ is the evaporation rate (g/s), m_d the droplet mass (g), τ_e the evaporation time (s) in the continuum region, where the droplet size is much larger than the gas mean free path, λ ($Kn = \lambda / d_d \ll 1$). τ_e can be calculated based on the following equation.⁵

$$\tau_e = \frac{R\rho_d D_d^2}{8D_g M \left(\frac{P_d}{T_d} - \frac{P_\infty}{T_\infty} \right)} \quad (2)$$

where D_d is droplet diameter (m), R is the gas constant, ρ_d is the droplet density (kg/m^3), D_g is the gas-phase diffusion coefficient of the solvent (as a function of furnace temperature, T_f), M is the molecular weight of the solvent (g/mol), T_∞ is the temperature far from the droplet (K), T_d is the temperature at the surface of the droplet (K) and becomes constant (= water boiling point) if the furnace temperature is larger than 100°C , P_∞ is the partial pressure of the solvent far from the droplet and can be neglected if dry gas is used (Pa), and P_d is the vapor pressure at the droplet surface (Pa). Combining equations (1) and (2), we get the following equation

$$D_d = \frac{3RkT_d}{4\pi D_g M P_d} \quad (3)$$

The mass density of a folded spherical graphene oxide particle, ρ , follows a scaling equation:⁶

$$\rho = \rho_m \left(\frac{F}{Yh} \right)^{\delta D} \left(\frac{D_p}{2h} \right)^{D-3} \quad (4)$$

where ρ_m is density of GO (1800 kg/m^3),⁷ Y is the two-dimensional Young's modulus (145.32 N/m for a single GO sheet with a thickness of 0.7 nm),⁸ D_p is the mobility diameter (nm), h is the GO thickness (0.7 nm for single sheet GO), δ is the force scaling exponent for a self-avoiding sheet (0.25),⁹ and D is the characteristic fractal dimension of GO (2.54).¹⁰ The characteristic fractal dimension for any thin sheet material is independent of the bending rigidity as well as applied boundary conditions (e.g. confinement force and load rate).⁹

On the other hand, the particle diameter of a GO crumpled particle can also be calculated following one-droplet-to-one-particle (ODOP) principle based on mass conservation:^{11,12}

$$D_p = D_d \left(\frac{C}{\rho} \right)^{1/3} \quad (5)$$

where D_p and D_d are particle and droplet diameters (nm), respectively, C is the mass concentration (kg/m^3), and ρ is the mass density of a GO crumpled particle.

Combining equations (4) and (5), yields the following equation for confinement force:

$$F = Yh \left[\frac{C}{\rho_m} \left(\frac{D_d}{D_p} \right)^3 \left(\frac{D_p}{2h} \right)^{3-D} \right]^{1/\delta D} \quad (6)$$

The above equation can be further simplified into the follow form.

$$F = AC^{1/\delta D} D_p^{-1/\delta} D_d^{3/\delta D} \quad (7)$$

where A is constant ($A = Y2^{\frac{D-3}{\delta D}} h^{1+\frac{D-3}{\delta D}} \rho_m^{-\frac{1}{\delta D}}$). D_d in equation 7 can be replaced by equation 3, which yields the new equation of the confinement force.

$$F = AC^{1/\delta D} D_p^{-1/\delta} \left(\frac{3\kappa RT_d}{4\pi D_g M P_d} \right)^{3/\delta D} \quad (8)$$

Equation 8 can be further simplified into the following equation.

$$F = ABC^{1/\delta D} D_p^{-1/\delta} (\kappa T_d / P_d D_g)^{3/\delta D} \quad (9)$$

where B is constant ($B = (3R / (4\pi M))^{3/\delta D}$). In this work, the furnace temperature is always higher than 100°C, thus T_d and P_d become constant as well. From the above equation, one can find that the confinement force, F is propositional to mass concentration of precursor ($F \propto C^{1.57}$) and the evaporation rate and temperature ($F \propto \kappa^{4.72}$), but inversely propositional to particle diameter ($F \propto D_p^{-4}$). At a fixed precursor concentration and droplet size, evaporation rate (furnace temperature) becomes the only variable.

S3. Calculation of Residence Time

The residence time inside a diffusion dryer ($L = 33$ cm, $I.D. = 6$ cm) can be estimated using the following equation:

$$\tau_r = \frac{nV_{dryer}}{Q_g} \quad (10)$$

where n and V_{dryer} are the number and volume of the diffusion dryer (m^3), respectively, and Q_g is the gas flow rate (m^3/s). The residence times at 14 psi and room temperature ($Q_g = 2.06 \times 10^{-4} m^3/s$) are calculated as 0.20 s a single diffusion dryer and 0.40 s for two diffusion dryers, which are much longer than the corresponding evaporation time (5.08×10^{-3} s). Based on the above calculation results, it seems that using one or two diffusion dryers should be the same since all water evaporated within 0.01 s. It should be noted that the estimation of the evaporation time is based on single droplet evaporation without considering the effects of population (number concentration) of droplets and gas flow rate. The actual evaporation times of droplets in this work may be longer than the calculated ones. This is also the reason for the different results obtained for using different diffusion dryers.

S4. pH Effect

To control the processes of exfoliation, dispersion, functionalization, and self-assembly of suspended GO nanosheets in aqueous media, a fundamental understanding of their solution behavior is also necessary.¹³ In this sense, pH is another important parameter to be considered that is closely related to the physiological activity of GO aqueous suspension.^{3, 14} The pH-dependent hydrophilicity of GO has been exploited to control its assembly behavior.¹⁵ Recent analyses indicated that the peripheral carboxyl groups (-COOH) play a key role in determining the solution behavior of GO.^{16, 17} The colloidal stability of aqueous GO solutions has been attributed to the electrostatic repulsions between ionized carboxyl groups,¹⁶ which can be interpreted by measuring their zeta potential.^{18, 19} As seen in **Fig. S5a**, the dramatic change in the zeta potentials of GO aqueous suspensions at pH 1 and 12 reflects the fact that the edge carboxyl groups are highly protonated at pH 1 resulting in weak electrostatic repulsive forces. However, in pH 12, zeta potential was achieved as high as -45 mV. The corresponding hydrodynamic diameters of GO nanosheets measured by DLS also showed similar trend as zeta potential. These findings suggest that the electrostatic repulsions between ionized carboxyl groups at the GO nanosheet edges provide the major barrier preventing the GO sheets from aggregating.^{16, 20} Optical properties of the GO suspensions were also measured by UV-Vis spectroscopy as shown in **Fig. S5b**, where two characteristic absorption peaks of GO were observed at 230 nm and 300 nm originating from π - π^* transition of the C=C band and n - π^* transition of the C=O band, respectively.²¹ The pH-dependent absorption spectra of GO colloids suggest that the change in the concentration of H⁺ and OH⁻ causes the electronic transition changes of π - π^* and n - π^* in GO refilling or depleting their valence band.^{3, 22} Thus the protonation and deprotonation of carboxylate GO due to changes in pH may cause electrostatic doping/charging to the GO, thereby shifting the Fermi level similar to carboxylate SWCNTs.^{22, 23} However, the absorption spectrum is also affected by the solvent in which the absorbent species are dissolved in. By changing the pH, we can alter the polarization forces between the solvent and the absorber. At low pH, the solvent is abundant with positively charged hydrogen ions, while at high pH, the solvent is abundant with negatively charged hydroxide ions.²⁴ Thus, lowering the pH of the GO solution will increase the polarization forces between the GO (of negative zeta potential) with the positively charged hydrogen ions. This lowers the energy levels of both the π and π^* state. However, because the effect is greater for the excited state, the gap between the π and π^* orbitals is reduced—thus causing a redshift in the spectra. However, there is no significant size and morphology variation of crumpled GO particles prepared from GO aqueous solutions with different pH based on electron microscopy analysis (**Fig. 4**) and SMPS measurements (**Fig. S6**). The reason may be due to the lower magnitude of electric repulsive force as compared to the corresponding confinement force, which needs further investigation in the near future.

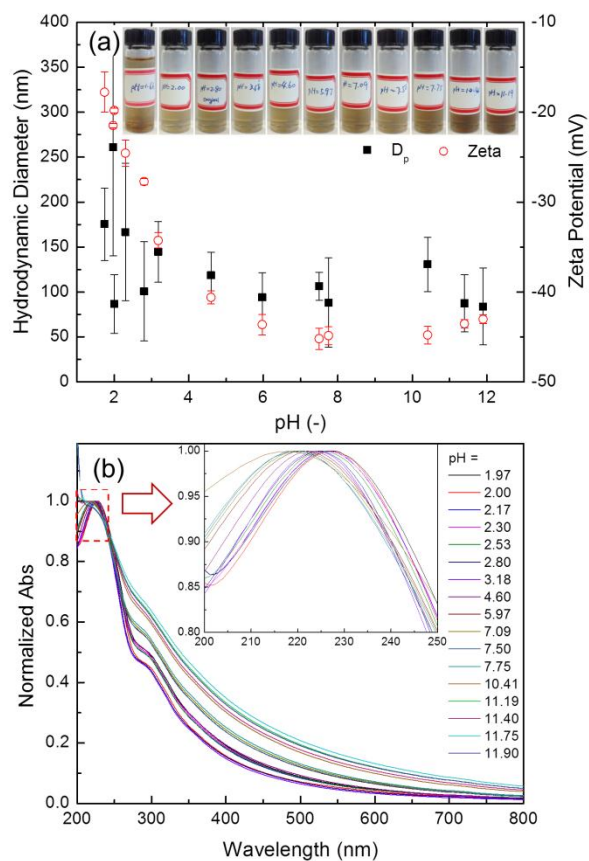


Figure S5. pH effect on the size and surface properties of graphene oxide. (a) Dynamic particle diameter and zeta potential, and (b) UV-Vis spectra of graphene oxide as a function of pH.

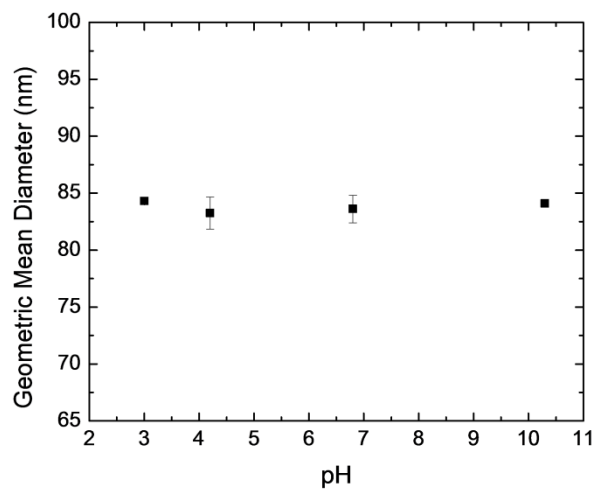


Figure S6. pH effect on the particle size of crumpled GO particles measured by SMPS.

Table S1. Effect of synthesis temperature with different diffusion dryers ($C = 0.3$ mg/ml, $P_{neb} = 96.53$ kPa).

Furnace temperature (°C)	Particle diameter	Confinement force	Particle diameter	Confinement force	Particle diameter	Confinement force
	_0dryer ^b (nm)	_0dryer ^c (μN)	_1dryer ^b (nm)	_1dryer ^c (μN)	_2dryers ^b (nm)	_2dryers ^c (μN)
200	88.22±0.49	29.75±0.66	87.36±0.12	30.94±0.17	89.16±0.39	28.52±0.50
400	84.32±0.16	34.87±0.26	86.39±0.37	31.65±0.55	87.42±0.60	30.18±0.81
600	83.40±0.77	37.80±1.40	84.49±0.24	35.89±0.40	85.53±0.27	34.18±0.43
800	80.99±0.88	41.58±1.76	82.22±0.72	39.14±0.36	85.50±0.33	33.47±0.51
1000	75.14±1.70	56.23±5.10	83.35±0.15	37.14±0.26	85.18±0.31	34.05±0.50

Table S2. Effect of precursor concentration ($T_f = 400^\circ\text{C}$, $P_{neb} = 96.53$ kPa)

Precursor concentration (mg/ml)	Droplet size (μm)	Evaporation rate (g/s)	Evaporation time (s)	Particle diameter (nm)	Confinement force (μN)
0.0375				78.09±0.21	47.40±0.51
0.1	2.82±0.06	7.88×10^{-7}	1.49×10^{-5}	81.95±0.17	39.08±0.32
0.3				84.32±0.16	34.87±0.26

S5. Supplementary References:

1. Hummers, W. S.; Offeman, R. E. *J Am Chem Soc* **1958**, 80, (6), 1339.
2. Atkins, P.; de Paula, J., *Atkins' Physical Chemistry*. 8th ed.; Oxford University Press: 2006.
3. Chen, J. L.; Yan, X. P. *Chem Commun* **2011**, 47, (11), 3135-3137.
4. Fuchs, N. A., *Evaporation and Droplet Growth in Gaseous Media*. Pergamon Press: London, 1959.
5. Hinds, W. C., *Aerosol Technology: Properties, Behavior, and Measurement of Airborne Particles*. Second ed.; John Wiley & Sons, Inc.: New York, 1999.
6. Balankin, A. S.; Silva, I. C.; Martinez, O. A.; Huerta, O. S. *Phys Rev E* **2007**, 75, (5), 051117.
7. Dikin, D. A.; Stankovich, S.; Zimney, E. J.; Piner, R. D.; Dommett, G. H. B.; Evmenenko, G.; Nguyen, S. T.; Ruoff, R. S. *Nature* **2007**, 448, (7152), 457-460.
8. Suk, J. W.; Piner, R. D.; An, J. H.; Ruoff, R. S. *Acs Nano* **2010**, 4, (11), 6557-6564.
9. Vliegthart, G. A.; Gommer, G. *Nat Mater* **2006**, 5, (3), 216-221.
10. Ma, X. F.; Zachariah, M. R.; Zangmeister, C. D. *Nano Lett* **2012**, 12, (1), 486-489.
11. Wang, W. N.; Widiyastuti, W.; Lenggoro, I. W.; Kim, T. O.; Okuyama, K. *J Electrochem Soc* **2007**, 154, (4), J121-J128.
12. Wang, W. N.; Kaihatsu, Y.; Iskandar, F.; Okuyama, K. *Chem Mater* **2009**, 21, (19), 4685-4691.
13. Dreyer, D. R.; Park, S.; Bielawski, C. W.; Ruoff, R. S. *Chem Soc Rev* **2010**, 39, (1), 228-240.
14. Shih, C. J.; Lin, S. C.; Sharma, R.; Strano, M. S.; Blankschtein, D. *Langmuir* **2012**, 28, (1), 235-241.
15. Eda, G.; Fanchini, G.; Chhowalla, M. *Nat Nanotechnol* **2008**, 3, (5), 270-274.
16. Li, X. L.; Zhang, G. Y.; Bai, X. D.; Sun, X. M.; Wang, X. R.; Wang, E.; Dai, H. J. *Nat Nanotechnol* **2008**, 3, (9), 538-542.
17. Lurf, A.; He, H. Y.; Forster, M.; Klinowski, J. *J Phys Chem B* **1998**, 102, (23), 4477-4482.
18. Ohshima, H., *Theory of Colloid and Interfacial Electric Phenomena*. Elsevier Academic Press: Amsterdam, 2006.
19. Hunter, R. J., *Zeta Potential in Colloid Science: Principles and Applications*. Academic Press: New York, 1981.
20. Hasan, S. A.; Rigueur, J. L.; Harl, R. R.; Krejci, A. J.; Gonzalo-Juan, I.; Rogers, B. R.; Dickerson, J. H. *Acs Nano* **2010**, 4, (12), 7367-72.
21. Clark, B. J.; Frost, T.; Russell, M. A., *UV Spectroscopy: Techniques, Instrumentation, Data Handling/UV Spectrometry Group*. Chapman & Hall: New York, 1993; Vol. 4.
22. Strano, M. S.; Huffman, C. B.; Moore, V. C.; O'Connell, M. J.; Haroz, E. H.; Hubbard, J.; Miller, M.; Rialon, K.; Kittrell, C.; Ramesh, S.; Hauge, R. H.; Smalley, R. E. *J Phys Chem B* **2003**, 107, (29), 6979-6985.
23. Zhao, W.; Song, C. H.; Pehrsson, P. E. *J Am Chem Soc* **2002**, 124, (42), 12418-12419.
24. Palanna, O. G., *Engineering Chemistry*. Tata McGraw Hill Education Pvt, Ltd.: New Delhi, 2009.